Somashekhar S Hiremath*, Arnab Gupta, Ankit Amin T and Ramakrishnan S

Investigation on surface properties of laser-textured Ti-6Al-4V ELI biomaterial

https://doi.org/10.1515/cdbme-2024-2074

Abstract: In this paper, a thorough analysis of nanosecond laser texturing on Ti-6A1-4V ELI material was carried out, with a particular emphasis on the modulation of laser process parameters and their effects on surface morphology, elemental composition, microscale topographical features, and wettability. The laser-textured samples exhibit unique surface morphologies that were identified by different topographical metrics such as average surface roughness (Sa), surface development ratio (Sdr), peak-to-peak distance (dp), and peak-to-valley height (hp) along parallel and perpendicular to laser scanning directions. The energy dispersive x-ray spectroscopy (EDS) was used to examine the differences in elemental composition and crystallographic constitution of the samples revealed using the x-ray diffraction analysis (XRD). Further contact angle measurement in both the parallel and perpendicular directions revealed the hydrophobicity of the laser-textured surfaces. Out of 4 samples, LT-2 and LT-4 samples displayed noticeably larger contact angles, demonstrating a high degree of hydrophobicity in both directions. Improved hydrophobicity of the textured surfaces may lead to reduced bacterial attachment, whereas anisotropic surface features at the microscale may provide contact guidance to osteoblast cells, opening up avenues for regenerative tissue engineering on biomaterial interfaces.

Keywords: Biomaterial, Ti-6A1-4V ELI, laser texturing, surface roughness, wettability, surface free energy.

1 Introduction

Dental and orthopaedic implants have made significant progress in recent years and have had a significant economic impact, but they still have a limited lifespan of 10–15 years in the body, and problems such as inflammation, infection, corrosion, wear, fracture, and lack of osseointegration can still occur [1]. Implant surfaces that do not integrate properly with the surrounding tissues are vulnerable to micromotion, which can eventually lead to implant loosening. Bacterial infections, with Staphylococcus aureus being the most common pathogen found in surgical wounds worldwide, are a leading cause of critical infections that can prevent proper implant integration and lead to joint and bone destruction. The role of nanoscale surface finish and anisotropic wettability produced using unidirectional abrasive flow finishing process on the attachment of Escherichia coli and Staphylococcus aureus on to Ti-6Al-4V ELI and SS 316L biomaterial was elaborate in recent study [2]. The need for dental and orthopaedic implants with enhanced biological responses is ever-present. To achieve significant improvements in the biological response of implants, higher surface functionality must be imparted, and using nano- and micro-structured implant surfaces is among the most promising approaches. Nano- and microstructured surfaces are expected to elicit a response from cells since they exist in a nano-structured environment in vivo and their machinery is composed of nano- and microstructures [3]. The properties of an implant, such as its surface roughness, anisotropy, wettability, and surface free energy, which are defined by its surface topography and chemical composition, play a critical role in controlling implant-host interactions following implantation. These interactions, such as water shell formation, protein absorption, cell adhesion, proliferation, and differentiation, are necessary for the formation of a solid implant-bone interface and to reduce the risk of infection [4].

2 Materials and Methods

The Ti-6Al-4V ELI sheet was sectioned into 10 mm x 10 mm x 1 mm coupons and polished successively, followed by ultrasonication to remove debris and any adhered contaminants. Further, these samples were textured using a Ytterbium (Yb)-fiber nanosecond pulsed laser system having main specification 50 W maximum power, 1045 nm wavelength, 50 kHz repetition rate, 30 μm beam spot diameter and 300 ns pulse duration. Table 1 shows four different Ti-6Al-4V ELI coupons processed under varied laser parameters, namely pulse energy (Ep), scanning speed (Vs), and hatch distance (H). These parameters were chosen based on a pilot study conducted with 36 different parametric conditions and favorable results are presented here. The respective samples were analyzed by a scanning electron

*Corresponding author: Somashekhar Hiremath : Indian Institute of Technology Madras, Chennai-600036. Tamil Nadu, India, e-mail: somashekhar@zmail.iitm.ac.in

Arnab Gupta, Ankit Amin, Ramakrishnan S: Indian Institute of Technology Madras, Chennai-600036. Tamil Nadu, India,

microscope (SEM) (INSPECT-F50) to investigate the effect of laser ablation on the surface morphology of the samples. The EDS was used to determine the surface elemental composition of the samples. To investigate the phase constitution, the samples were characterized using thin film XRD (Rigaku Smart Lab, Japan) employed with Cu-Kα radiation of wavelength 0.154 nm.

Table 1: Laser surface processing parameters.

Samples	Pulse Energy, Ep (μJ)	Scanning Speed, Vs (mm/s)	Hatch distance, H (μm)
LT-1	20	600	15
LT-2	20	600	30
LT-3	20	1000	30
LT-4	50	600	30

The Bragg angle range was fixed at 20°–80° with a 3° per minute scanning speed. Non-contact optical profilometry was carried out using a 3D optical profilometer (Bruker Nano GmbH). A sampling area of 150 μm x 150 μm was selected for analysis on each surface, and the 3D and 2D reconstruction was carried out using image processing Mountains®9 software. The areal surface parameters such as Sa, Sdr, dp and hp distances were also determined from the generated 2D profiles. Further, the evaluation of wettability was used to ascertain the contact angle using a contact angle goniometer (DSA25KRUSS GmbH) with a precisely dispensed 5 μl droplet of de-ionized water, and three readings were recorded at room temperature. To evaluate the surface free energy of the respective samples, contact angles subtended by DI water, formamide, and diiodomethane are recorded following the same procedure as above. Table 2 shows the surface tension components of the different testing liquids at 20°C [2].

Table 2: Surface tension components (mN/m) of testing liquids

Liquids	γ_l	γ_l^{LW}	γ_l^{AB}	γ_l^{+}	γ_l^{-}
Diiodomethane	50.8	50.8	≈ 0	≈ 0	≈ 0
Formamide	58	39	19	2.28	39.6
DI water	72.8	21.8	51	25.5	25.5

Then, using the Van-Oss-Chaudhary-Good equation (eq. 1), the dispersive (Van der Waal's component) and polar (acid-base component) surface free energies were calculated using the following equations [2].

$$\frac{(1+\cos\theta)\gamma_l}{2} = \sqrt{\gamma_s^{LW}\,\gamma_l^{LW}} + \sqrt{\gamma_s^{+}\,\gamma_l^{-}} + \sqrt{\gamma_s^{-}\,\gamma_l^{+}} \quad \textbf{(1)}$$

$$\gamma_s^{AB} = 2\sqrt{\gamma_s^{+}\,\gamma_s^{-}} \quad \textbf{(2)}$$

$$\gamma_s^{total} = \gamma_s^{LW} + \gamma_s^{AB} \quad \textbf{(3)}$$

Where, γ^{LW} is dispersive component accounting for Liftshitz Van der Waal's interactions

γ^{AB} is polar component accounting for acid-base or donor-acceptor type interactions

γ^{+} is Lewis-acid component, electron acceptor

γ^{-} is Lewis-base component, electron donor

Subscript *s* and *l* denotes solid surface and liquid surface

3 Results and Discussions

Figure 1 shows the SEM micrographs of polished and laser-textured samples. The LT-1 reveals fishbone (alternative V-shaped) type of micro-morphology originating due to high pulse as well as line overlap, whereas crescent-shaped repeatable micro textures are visible in LT-2 and LT-4 because of relatively lower line overlap. In LT-4, a higher pulse energy distribution leads to periodic micro-bulges along the laterally overlapped laser scanning lines in addition to thicker crescent-shaped ridges along the laser scanning direction. Sparsely distributed ring-type structures are observed in LT-3 due to relatively lower pulse overlap.

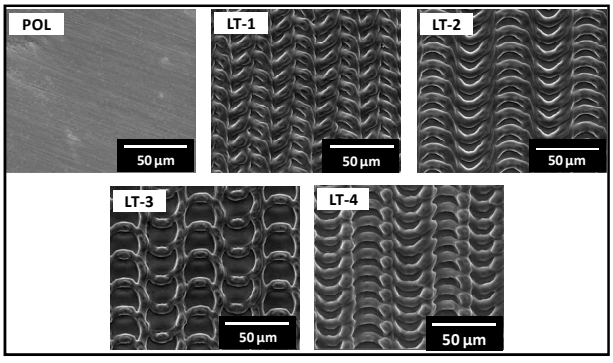

Figure 1: SEM images of the laser textured samples

The laser texturing (LT) process parameters have a significant impact on the surface topography, as inferred from the values of Sa and Sdr obtained through 3D optical profilometry-based surface reconstruction as shown in Figure 2. The laser-textured samples exhibit enhanced surface roughness and the surface development ratio as compared to polished surfaces. LT-2 reveals the highest Sa and Sdr values of 1.9 μm and 41.27%, followed by LT-4, LT-3, and LT-1, respectively, in the order. From the established literature, an improved Sa and Sdr is conducive to better osteoblast

attachment and proliferation [3]. Among the collected samples, LT-2 exhibited the highest disparity in both the peak-to-peak and peak-to-valley height distances in both directions, indicating a greater degree of anisotropy compared to the other samples. Additionally, LT-4 demonstrated favorable anisotropic properties when compared to LT-1 and LT-3. Hence, these two samples displayed superior anisotropy characteristics compared to the remaining samples, making them more desirable for further analysis and potential applications in tissue engineering.

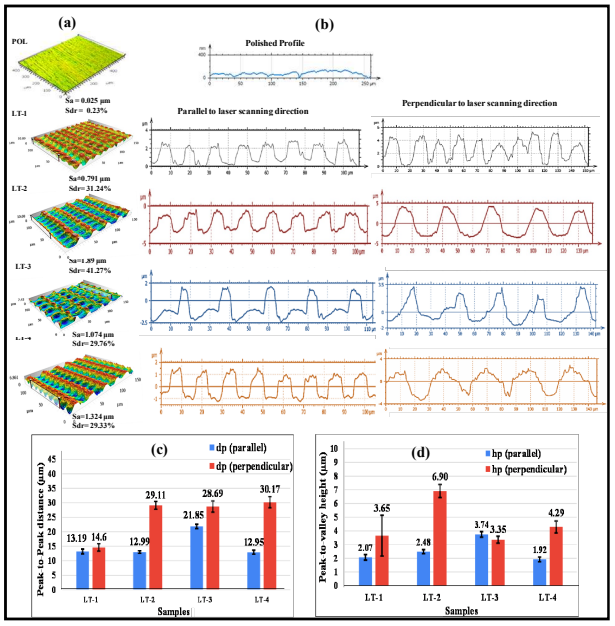

Figure 2: Optical profilometry results a) 3D surface profiles b) Depth-wise 2D reconstructed profilometry data c) Peak-to-peak distance d) Peak-to-valley height.

Figure 3 reveals the surface elemental composition of the textured surfaces at different locations, namely at the ridges and valleys. Laser ablation in atmospheric conditions leads to the formation of different metallic oxides on the surface, predominantly titanium oxides. Therefore, it is observed that there is an increase in oxygen percentage in the overall area for all the samples compared to the polished surface. However, it may be observed that at different regions on the textures, such as the peaks (R1), troughs (R2) along the texture direction, and overlapping boundaries (R3) perpendicular to the texture direction, the elemental comparison varies. When the laser is focused on a particular spot, the metal in that region converts into a molten state due to the very high temperature, and there is the flow of molten metal around the plume to the surface due to the temperature-induced surface energy gradient in the nearby region, and thus ridges are reformed as molten metal is accumulated. This flow of molten metal is also known as Marangoni's flow. The pressure applied by the gaseous plume on the molten metal pool at the laser-focused region also ejects the molten metal outwards. Molten metal is highly reactive and readily reacts with atmospheric oxygen to form metallic oxides, predominantly titanium oxides (TiOx). This resolidifies to form micro-bulges in the form of ridges, as observed in region R. This leads to higher oxygen concentration at the ridges and overlapping regions (R1 and R3) as compared to the trough (R2). Also, by changing the laser process parameters for LT-1, LT-2, and LT-4, not much variation in oxygen content is visible. However, for LT-3, the oxygen content is slightly less, which may be attributed to the lower spatial density of oxide-rich ridges.

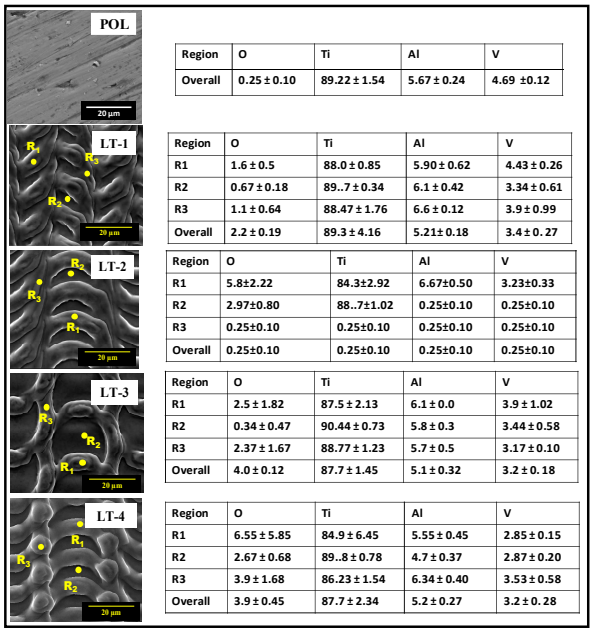

Region	O	Ti	Al	V
Overall	0.25 ± 0.10	89.22 ± 1.54	5.67 ± 0.24	4.69 ±0.12

Region	O	Ti	Al	V
R1	1.6 ± 0.5	88.0 ± 0.85	5.90 ± 0.62	4.43 ± 0.26
R2	0.67 ± 0.18	89..7 ± 0.34	6.1 ± 0.42	3.34 ± 0.61
R3	1.1 ± 0.64	88.47 ± 1.76	6.6 ± 0.12	3.9 ± 0.99
Overall	2.2 ± 0.19	89.3 ± 4.16	5.21± 0.18	3.4 ± 0. 27

Region	O	Ti	Al	V
R1	5.8±2.22	84.3±2.92	6.67±0.50	3.23±0.33
R2	2.97±0.80	88..7±1.02	0.25±0.10	0.25±0.10
R3	0.25±0.10	0.25±0.10	0.25±0.10	0.25±0.10
Overall	0.25±0.10	0.25±0.10	0.25±0.10	0.25±0.10

Region	O	Ti	Al	V
R1	2.5 ± 1.82	87.5 ± 2.13	6.1 ± 0.0	3.9 ± 1.02
R2	0.34 ± 0.47	90.44 ± 0.73	5.8 ± 0.3	3.44 ± 0.58
R3	2.37 ± 1.67	88.77 ± 1.23	5.7 ± 0.5	3.17 ± 0.10
Overall	4.0 ± 0.12	87.7 ± 1.45	5.1 ± 0.32	3.2 ± 0. 18

Region	O	Ti	Al	V
R1	6.55 ± 5.85	84.9 ± 6.45	5.55 ± 0.45	2.85 ± 0.15
R2	2.67 ± 0.68	89..8 ± 0.78	4.7 ± 0.37	2.87 ± 0.20
R3	3.9 ± 1.68	86.23 ± 1.54	6.34 ± 0.40	3.53 ± 0.58
Overall	3.9 ± 0.45	87.7 ± 2.34	5.2 ± 0.27	3.2 ± 0. 28

Figure 3: Surface elemental composition of the polished and textured samples at different locations.

Figure 4 depicts the XRD patterns of the laser-textured sample in contrast with the untreated surface (POL).

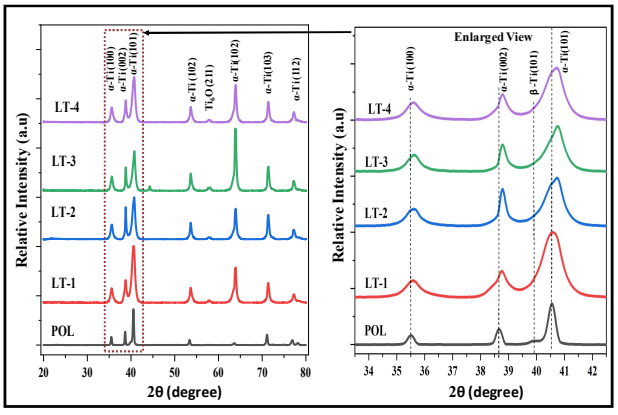

Figure 4: XRD patterns of the sample.

From the Figure, α-Ti (hexagonally closed packed) is seen to be the dominant phase, with peaks observed at 35.5° (100), 38.6° (002) and 40.5° (101), whereas β-Ti phase in vestige could be ascertained from the convoluted peak at 39.8° (110), as observed in the magnified spectrum of 20 range 34°-42° in Figure 4 (b).

Evolved Ti_6O oxide phase could be observed from the peak at 58° (006) for LT-1, LT-2, LT-3, and LT-4 samples. It is also observed that in LT-3, Ti_6O has two peaks, one at 42° (104) and 58° (006) that indicates a higher presence of the oxide phase.

Figure 5 shows the contact angle measured in both parallel and perpendicular directions of the surfaces along with the mean surface free energy components.

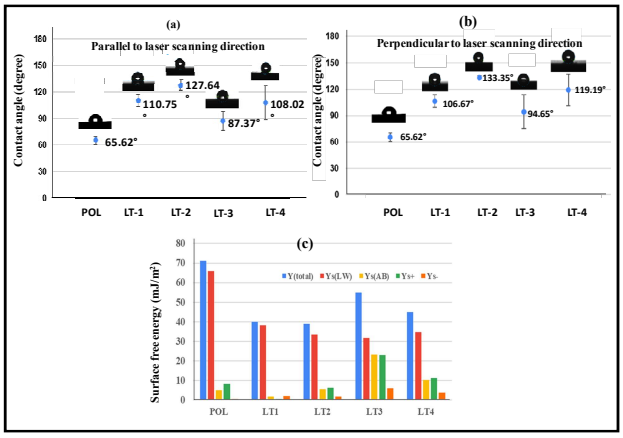

Figure 5: Contact angle of the samples and mean surface free energy components.

The polished sample exhibits a contact angle of 65.62° in both the perpendicular and parallel directions, which indicates that the surfaces exhibit moderate hydrophobicity. Sample LT-1, the contact angles of 106.67° (perpendicular) and 110.75° (parallel), suggest that the surface is more hydrophobic compared to the polished sample. For LT-2, the contact angles of 133.35° (perpendicular) and 127.84° (parallel) indicate a highly hydrophobic surface. For LT-3, the contact angles of 94.35° (perpendicular) and 87.37° (parallel) suggest that the surface is less hydrophobic.

For LT-4, the contact angles of 119.19° (perpendicular) and 108.02° (parallel) indicate a relatively high level of hydrophobicity.

In summary, the laser texturing process has generally increased the hydrophobicity of the Ti-6Al-4V ELI material in both the perpendicular and parallel directions. Improved hydrophobicity of the textured surfaces may tend to reduce the bacterial attachment, whereas anisotropic surface features at microscale may provide contact guidance to osteoblast cells, opening up avenues for regenerative tissue engineering on biomaterial interfaces.

4 Conclusions

In the current study, the influence of nanosecond laser texturing parameters on the physicochemical properties of Ti-6A1-4V ELI material was examined. The laser process parameters, including hatch distance, scanning speed, and pulse energy, were adjusted to create different surface textures. The surface properties were primarily influenced by factors such as pulse overlap and line overlap. Each sample exhibited distinct surface morphologies and chemistry, as indicated by average surface roughness (Sa), surface development ratio (Sdr), peak-to-peak distance (dp), and peak-to-valley height (hp) along both directions and similarly in distinct elemental and phase constitutions. Among the four surfaces exhibiting visible periodic anisotropy, LT-1 sustained noticeably higher anisotropy in both the dp and hp measurements within its micro-scaled features. The surfaces treated with laser texturing displayed hydrophobic properties in both the parallel and perpendicular directions to the laser scan direction (LSD). This hydrophobic behavior indicates that the laser textured surfaces repel water, preventing it from easily spreading or adhering to the surface. Among the LT surfaces, LT-2 exhibited the highest contact angle and the lowest surface energy. These insights can be valuable for applications that require surfaces with lower bacterial adhesion and contact guidance for mammalian cell proliferation.

Author Statement

Research funding: The author state no funding involved. Conflict of interest: Authors state no conflict of interest. Informed consent: Informed consent has been obtained from all individuals included in this study.

References

[1] Han, H. J., Kim, S., & Han, D. H. (2014). Multifactorial evaluation of implant failure: a 19-year retrospective study. International journal of oral & maxillofacial implants, 29(2).

[2] Kumar, S. S., Hiremath, S. S., Ramachandran, B., & Muthuvijayan, V. (2019). Effect of surface finish on wettability and bacterial adhesion of micromachined biomaterials. *Biotribology*, *18*, 100095.

[3] Ren, B., Wan, Y., Wang, G., Liu, Z., Huang, Y., & Wang, H.(2018). Morphologically modified surface with hierarchical micro-/nano-structures for enhanced bioactivity of titanium implants. Journal of Materials Science, 53(18), 12679-12691. Yang, Y., Cavin, R., & Ong, J. L. (2003). Protein adsorption on titanium surfaces and their effect on osteoblast attachment. Journal of Biomedical Materials Research Part A: An Official Journal of The Society for Biomaterials, The Japanese Society for Biomaterials, and The Australian Society for Biomaterials and the Korean Society for Biomaterials, 67(1), 344-349.